A Project Report

On

DESIGN AND SIMULATION FOR THE CONTROL OF SIX DEGREES OF FREEDOM DYNAMICS

BY

SAHIL KOMMALAPATI

15XJ1A0326

Under the supervision of

PROF. ABHIJIT BHATTACHARYYA

PROF. VIJAYSEKHAR CHELLABOINA

SUBMITTED IN PARTIAL FULLFILLMENT OF THE REQUIREMENTS OF

SE 422: PROJECT TYPE COURSE

MAHINDRA ECOLE CENTRALE

COLLEGE OF ENGINEERING

HYDERABAD

(APRIL 2019)

Acknowledgement

I would like to thank Prof. Vijaysekhar Chellaboina for enabling me to work in such an interesting field and constantly monitoring my progress through invaluable guidance and suggestions. I would also like to thank my mentor for the project, Prof. Abhijit Bhattacharyya for his continuous support throughout the duration of the project and teaching me the proper etiquette for scientific presentation and writing.

Table of Contents

List of symbols

F_N	Normal Force on the Missile
V_M	Missile Velocity along the Body axis
α	Angle of attack
θ	Angle of the missile w.r.t the reference axis
γ	Angle of the velocity vector w.r.t the reference axis
CP	Center of Pressure
CG	Center of Gravity
n_L	Missile Acceleration perpendicular to the body axis
n_B	Missile Acceleration perpendicular to the Velocity Vector
Q	Dynamic Pressure
C_N	Force Coefficient to F_N
C_M	Moment Coefficient to Moment along CP
π	Pi
d	The diameter of the Missile's body cylinder
δ	The surface deflection in the fin
β	Normalized speed coefficient
$Mach$	Mach number
M	Moment along the CP
W	Weight of the missile
I_{yy}	Moment of Inertia
g	Acceleration due to gravity

Abstract

One of the significant applications of control systems is in the field of defense research. In particular, the stability of any machinery is dependent on the design of the control system. In this project we look at one of such application: Intercontinental Ballistic Missiles. We begin with understanding the basics of flight control in missile and the different types of navigation techniques used to control the trajectory. A simple geometric model of the missile is assumed and a corresponding Transfer Function (TF) is developed to describe its motion. A simple navigational law called Proportional Navigational Law (PNL) is explored. An Introduction to Tail Based Navigation (TBN) is presented and a corresponding TF is designed to govern the trajectory of the missile. Since the preliminary step to testing the system design would be to simulate it virtually. Programs in MATLAB * and SIMULINK were developed. A comparative study on the differences between working on both the environments is also presented. A case study on the Rate Gyro Flight control system (RG FCS) and the Three Loop Autopilot flight control system (TLAP FCS) has been presented. The TLAP FCS is an advanced flight Control system which enables a superior control of the missile.

*

Commercial software is identified for the sake of completeness. This does not constitute endorsement of these products.

Chapter-1 Motivation and Background.

The field of control system is quite fascinating with its multifaceted applications. It is widely used to stabilize a desired output parameter of a system. It is extensively used in guiding the trajectory of air borne vehicles and in warfare. The use of efficient tactical guided missiles has their origin in Germany, prior to the world war and it has come a long way since its inception. A control system encompassing several essential components of flight governing the trajectory of the body is called as a Flight Control Strategy.

In this project, we work on a control system to control the missile path and study the important topics related to improving missile guidance system performance and understand the key design concepts and tradeoffs.

In particular, a modern control strategy called as the 'Three Loop Autopilot Flight Control Strategy' (TLAFCS) is studied and simulated. This study begins by understanding the basics of a flight control problem. Several assumptions which are made to simplify the study are understood and their impact in the actual replication of the problem is understood.

In order to completely comprehend the utility of TLAPFCS, we begin by studying simple navigational control laws, which were initially used before the Flight control systems were evolved to the complexity currently observed in the present day and age. The study and simulation of the older techniques act as building blocks in understanding the superiority of the current practices.

The three loop autopilot can be considered as an evolutionary control strategy. Since, its roots begin with a simple open loop FCS. This comprises of the most simplistic and irreplaceable components to design a FCS. It is simply an autopilot, an actuator and a missile transfer function connected in a straight forward open loop fashion. Hence, it is called as the Open Loop Flight Control Strategy. From this point onwards we try to build our TLAPFCS by adding numerous sensors through two stages of evolutions.

The entire report consists of understanding the role each part of the control system has in modifying the nature of the output. The Course on Control systems by Prof. Abhijit Bhattacharyya played a crucial role in understanding the basic terminology of the controls used while researching on various topics. The books Modern Control Theory by K.Ogata [1] and the tactical and strategic missile guidance by Paul Zarchan [2] played an important role in the background research.

Finally, Considering the evolutionary nature of the Three Loop Autopilot FCS, it is a better strategy to simulate them in Simulink than in Matlab script. Simulink is an environment in which highly visual block diagrams can be designed and simulated thus simplifying further modification and extensions. This enables us to use the previous block diagrams to work and expand on; effectively reducing the duplication of code and effort.

The next chapter describes the missile geometry and the assumptions which were made to simply the model. Establishing the geometry is the first step in undertaking the missile control problem, which will further be elucidated in the upcoming chapters.

Chapter-2 Missile geometry and physics

Introduction

The body of the missile is subjected to a great extent of research and occupies a position of great significance in the field of Fluid Mechanics, owing to the streamlining, flow field piercing and other optimization problems. But, since the topic of research in the current project is the design of a robust control system for stability analysis, we assume a rather simplified model for the geometry of the missile.

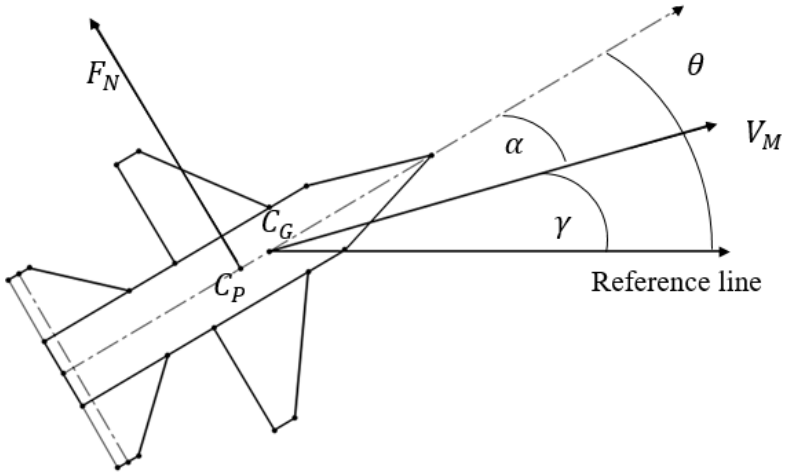

Figure 1: Model of the missile

In the Fig.1, the model assumes a cylindrical body, a cone shaped nose and four trapezoids for fins and tail respectively. This model simplifies the governing physics drastically, which would be further explored.

Tail based navigation

There are numerous methods of maneuvering a missile. By maneuvering it, we refer to the method in which we can we can control the future path of the missile. This problem could be further reduced to controlling the acceleration component (n_l) of the missile which is perpendicular to the body axis. This component is responsible for the amount of lift generated in the missile. A tail based navigation is implemented to observe the change in the n_l and then corresponding angle of attack (α). In the tail based navigation, as the name suggests, the tail of the missile, in particular the deflection caused in the tail of the missile about the hinge line and along the body axis of the missile, is used to govern the n_l of the body.

The physics governing the motion is quite elementary but arduous. The motion of the missile is governed by the force and the moment equation applied along the body of the missile. In these equation the geometry of the missile plays a huge role and the importance of a simplified model can be observed.

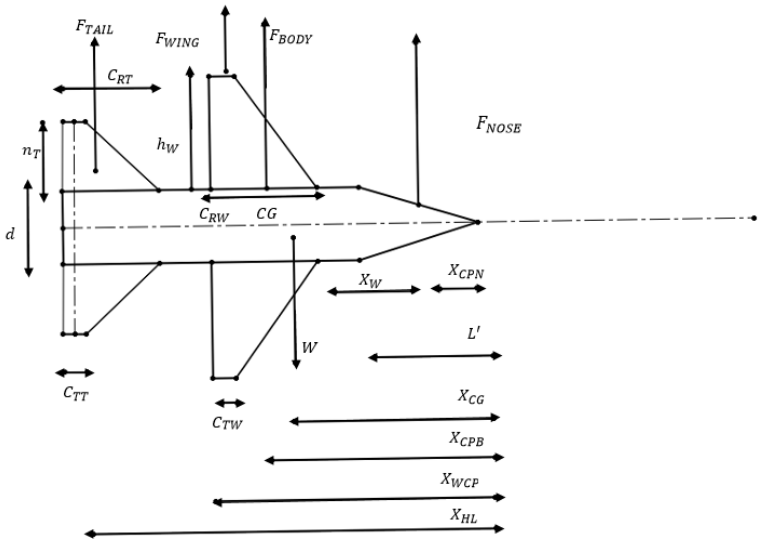

Figure 2: Side view of the model

Deriving the force equation governing the motion of the missile, we acknowledge the fact that the equivalent force acts through the Centre of Pressure (CP). The force equation can be written as

$$F = QS_{ref}C_N \tag{1}$$

$$Q = 0.5\,\rho V_M^2 \tag{2}$$

$$S_{ref} = \frac{\pi d^2}{4} \tag{3}$$

Here, the Q is the dynamic pressure and S_{ref} is the reference pressure and the C_N is the normal force coefficient. The normal force coefficient takes the different areas of the model (Fig.2) into consideration and accounts them in the force equation. The S_{ref} also acts a normalizing term for the normal force coefficient. Neglecting the interface effects between each part (the tail and the fin, the fin and the nose etc..) the Normal force coefficient can be written as [3]

$$C_N = 2\alpha + \frac{1.5S_{PLAN}\alpha^2}{S_{ref}} + \frac{8S_W\alpha}{\beta S_{ref}} + \frac{8S_T(\alpha+\delta)}{\beta S_{ref}} \tag{4}$$

Here, the contributions in the equation can be attributed to the nose, body, wing and the tail respectively. α is the angle of attack, δ is the angle of the deflection in the tail, which is given as an input into the transfer function; which is detailed in a further chapter. The S_{PLAN}, S_W, S_T refer to the reference areas of the planform, wing and tail respectively. Planform is the shape of the missile as viewed directly from above. Hence,

$$S_{PLAN} \approx Ld \tag{5}$$

The tails and the wings of missile are approximated as trapezoids, hence their reference areas

$$S_W = 0.5h_W(C_{TW} + C_{RW}) \tag{6}$$

$$S_T = 0.5h_T(C_{TT} + C_{RT}) \tag{7}$$

The parameter β is normalize speed, ($\sqrt{Mach^2 - 1}$); Mach = $\frac{V_{missile}}{V_{sound}}$.

In a similar manner the moment equation can also be derived. The moment is calculated as the normal force (F_N) multiplied by the moment arm. Here, it is to be noted than the coefficient of normal force will be modified to a moment coefficient.

$$M = (QS_{REF}C_M)d \tag{8}$$

$$C_M = 2\alpha\frac{X_{CG} - X_{CPN}}{d} + \frac{1.5S_{PLAN}\alpha^2}{S_{ref}}\frac{X_{CG} - X_{CPB}}{d} + \frac{8S_W\alpha}{\beta S_{ref}}\frac{X_{CG} - X_{CPW}}{d} + \frac{8S_T(\alpha + \delta\,)}{\beta S_{ref}}\frac{X_{CG} - X_{HL}}{d} \tag{9}$$

Here, the terms $X_{CG}, X_{CPN}, X_{CPB}, X_{CPW}, X_{HL}$ can be understood from Fig. 1.2. One important assumption which was made is that the X_{CG} is taken as 0.5 L for simplicity. Now, from the force and the moment equations we try to obtain the value of the the acceleration (n_l) and the angle of attack (α). Two equations and two unknowns can have a complete analytical solution.

The weight of the missile is taken as W, let g denote the acceleration due to gravity, and I_{yy} be the moment of inertia, then the required parameters can derived using the equations below to exhaustively predict the trajectory:

$$n_B = \frac{F_N g}{W} = \frac{gQS_{ref}C_M}{W} \tag{10}$$

$$\ddot{\theta} = \frac{M}{I_{yy}} = \frac{Q_{Sref}dC_M}{I_{yy}} \tag{11}$$

Here n_B is the body acceleration normal of the missile. In order to obtain the missile acceleration and the angle of attack, a simple understanding of the Fig.1 gives us the relation

$$\alpha = \theta - \gamma \tag{12}$$

To clarify, n_B is the acceleration of the missile perpendicular to the body and n_l is the acceleration of the missile perpendicular to V_m. Both of these terms are used interchangibly, owing to the small deflection in θ. Now, keeping this in mind the above equation can be written as

$$\alpha \coloneqq \dot{\theta} - \dot{\gamma} = \dot{\theta} - (\frac{n_L}{V_M}) \tag{13}$$

or approximately as,

$$\alpha \coloneqq \dot{\theta} - \dot{\gamma} = \dot{\theta} - (\frac{n_B}{V_M}) \tag{14}$$

Chapter-3 Missile Transfer Function

Introduction

A transfer function (TF) is a mathematical function which relates the desired parameter (the output) with the controllable parameters (the input). The internal working of the transfer function could be taken as a black box to simply understand the nature of the output. However, since the desired physics of the missile has been derived in the previous chapter, we now try to work out the transfer function for a tail based navigational control where the input is the angle of deflection in the tail and the outputs are the missile acceleration (η_l) and the angle of attack (θ). With the knowledge of these two parameters, we can successfully launch a missile and guide its towards a target.

From the above physics described in Chapter-2, a MATLAB code has been written to observe the output of the missile, for a constant tail deflection of 5°, travelling at a speed of 916 m/s and travelling at sea-level the output can be observed from Fig.3. The height at which the missile is travelling plays a role in determining the density of air, which is a function of altitude.

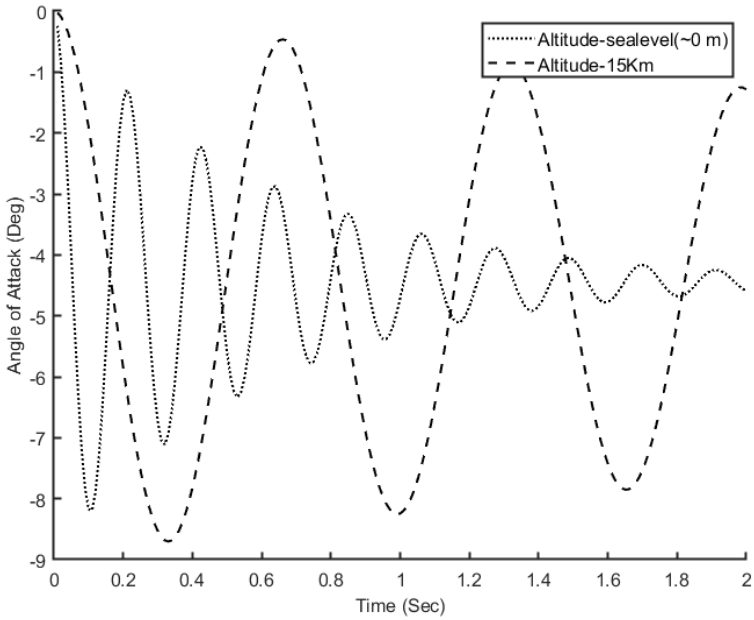

Figure 3: The Angle of attack over time

In the Fig.3, two plots have been show, which are drawn at sea-level and at an altitude of 15240m. It can be observed that the oscillations reach a steady state value quicker in the scenario where the missile is travelling at lower altitude. This result can be used a verification to the results of the transfer function which would be derived further. In order to simplify the formulation and reduce the computational burden regarding the TF, we linearize the prior force and moment equations.

Considering the fact that all of the parameters of interest, except for the angle of attack (α) are linear. This can be observed from the force and the moment coefficients where an α^2 can be observed. In order to get rid of this non-linearity, the coefficients are decomposed into terms which

are dependent on the δ and α saperately, Thus making each term independently linear. In the linearization process the force and the moment coefficients are modified as the following.

$$C_N = f(\alpha, \delta) = C_{N\alpha}\alpha + C_{N\delta}\delta \tag{15}$$

$$C_{N\alpha} = 2 + \frac{1.5S_{PLAN}\alpha}{S_{ref}} + \frac{8S_W}{\beta S_{ref}} + \frac{8S_T}{\beta S_{ref}} \tag{16}$$

$$C_{N\delta} = \frac{8S_T}{\beta S_{ref}} \tag{17}$$

Now, the missile truing rate can be expressed in a linearized form as,

$$\dot{\gamma} \approx \frac{n_L}{V_M} = \frac{gQS_{ref}}{WV_M}\left[C_{N\alpha}\alpha + C_{N\delta}\delta\right] = -Z_\alpha\alpha - Z_\delta\delta \tag{18}$$

Similarly, for the moment equations the moment coefficient can be decomposed as

$$C_M = f(\alpha, \delta) = C_{M\alpha}\alpha + C_{M\delta}\delta \tag{19}$$

where,

$$C_{M\alpha} = \frac{2(X_{CG} - X_{CPN})}{d} + \frac{1.5S_{PLAN}\alpha}{S_{ref}}\frac{X_{CG} - X_{CPB}}{d} + \frac{8S_W}{\beta S_{ref}}\frac{(X_{CG} - X_{CPW})}{d} + \frac{\frac{8S_T}{\beta S_{ref}}(X_{CG} - X_{HL})}{d} \tag{20}$$

$$C_{M\delta} = \frac{8S_T}{\beta S_{ref}}\frac{X_{CG} - X_{HL}}{d} \tag{21}$$

Now, the linearized missile angular acceleration can be expressed as,

$$\ddot{\theta} = \frac{M}{I_{yy}} = \frac{QS_{ref}d}{I_{yy}}\left[C_{M\alpha}\alpha + C_{M\delta}\delta\right] = M_\alpha\alpha + M_\delta\,\delta \tag{22}$$

where, (23)

$$M_\alpha = \frac{QS_{ref}dC_{M\alpha}}{I_{yy}}$$

$$M_\delta = \frac{QS_{ref}dC_{M\delta}}{I_{yy}} \tag{24}$$

Now, the overall Transfer Function can be simplified and written as

$$\frac{n_L}{\delta} = -\frac{V_M[M_\alpha Z_\alpha - Z_\alpha M_\delta]}{1845 M_\alpha} \frac{\left[1 - \frac{Z_\delta s^2}{M_\alpha Z_\delta - Z_\alpha M_\delta}\right]}{1 + \frac{Z_\alpha}{M_\alpha} s - \frac{s^2}{M_\alpha}} \tag{25}$$

where,

$$Z_\alpha = -\frac{gQS_{ref}C_{N\alpha}}{WV_M} \tag{26}$$

$$Z_\delta = -\frac{gQS_{ref}C_{N\delta}}{WV_M} \tag{27}$$

A block diagram can be drawn to better visualize the inner workings of the transfer function.

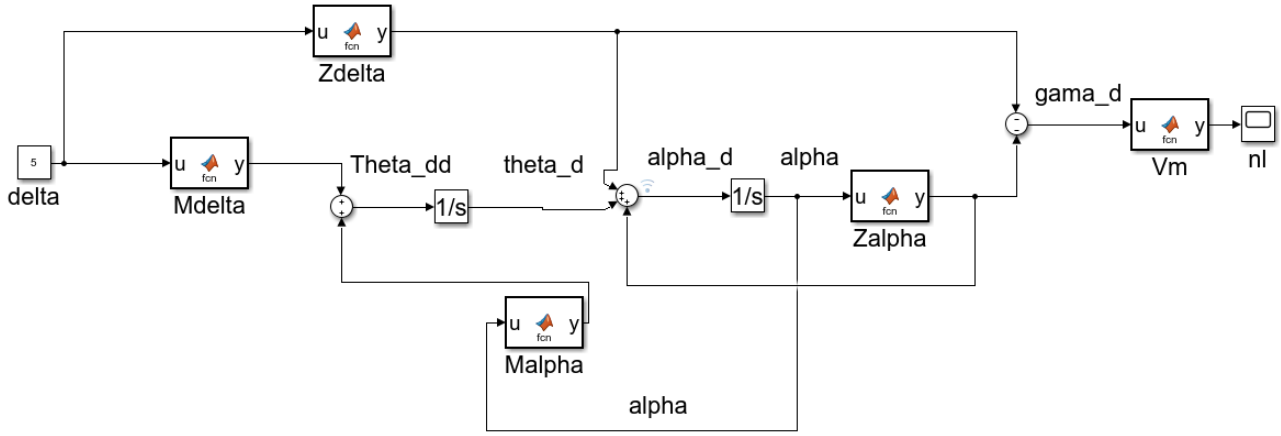

Figure 4: Linearized block diagram designed in SIMULINK

In the above block diagram (Fig. 4), the notation '_d' implies a derivative with respect to the terms preceding it. For example, the terms θ_d implies $\dot{\theta}$. The values of the block functions have been indicated above. The output of the scope which had a run time of 2s is shown below.

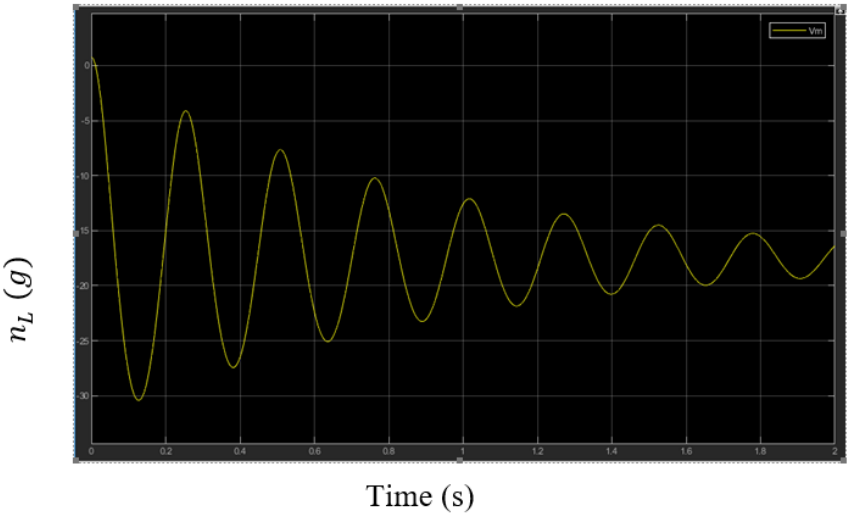

Figure 5: Missile acceleration over time (Linearized)

From Fig.4 It can also be observed that the signal of α can also be scoped out to observe its nature. The following plot shown in Fig.5 and Fig.6 depicts the same.

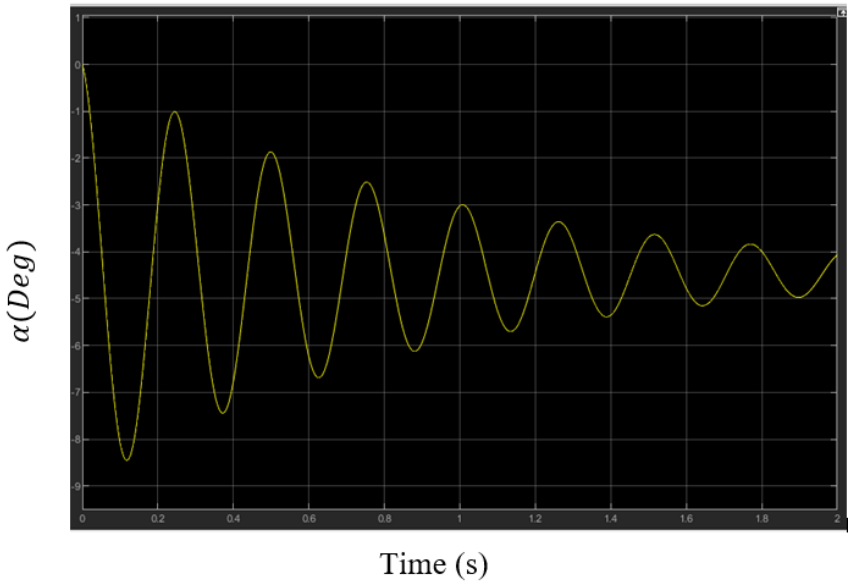

Figure 6: Missile angle of attack over 2s.

An Important note to be made in the process of linearization is that the because the equation for $C_{M\alpha}$ contains an alpha term, the equations (19) and (20) are still non-linear as they contain a $C_{M\alpha}\alpha$ terms associated with them . Hence, In order to approximate this non-linearity the α term in $C_{M\alpha}$ is calculated before using trim angle of attack conditions. At trim angle of attack, the moment coefficient is zero. Now, the equation (19) is solved for α_{trim} which is used in $C_{M\alpha}$ to linearize the transfer function.

In order to comprehend how the linearization approximated the output acceleration signal, a comparative plot has been generated, which can be observed below in Fig. 7(i). Here, it can be observed that both the output signals converge to a single steady state value of 12.97g.

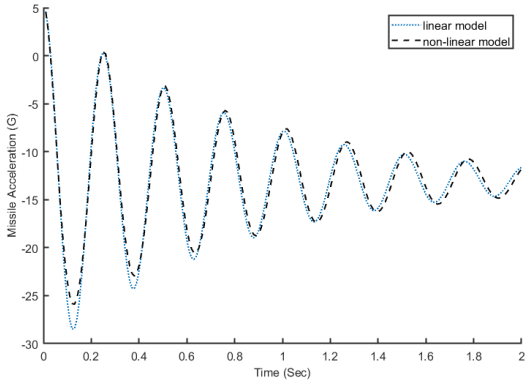

Figure 7(i): Linear and non-linear plots of missile acceleration.

In order to observe the steady-state values of both types of transfer functions, the simulations in Fig.7 have been extended to 12s and the following outputs (Fig. 7(ii)) have been obtained.

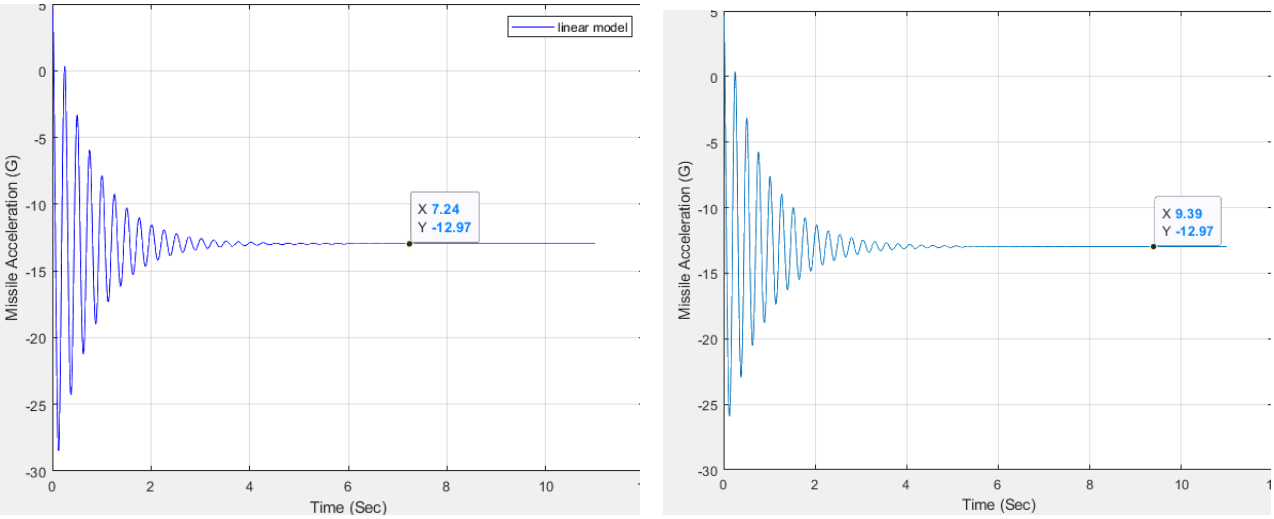

Figure 7(ii): Linear and non-linear plots of missile acceleration.

The transfer function of the missile takes the δ as the input and gives the n_L and α as the output. Where, the α can be obtained from the value of the $\dot{\theta}$. In order to simplify further representation of the TF, the following simplifications are done: (from eq. (25))

$$\frac{n_l}{\delta} = \frac{k_1\left(1 - \frac{s^2}{\omega_z^2}\right)}{1 + \frac{2\zeta_{AF}}{\omega_{AF}} + \frac{s^2}{\omega_{AF}^2}} \tag{28}$$

Where,

$$k_1 = -\frac{V_M[M_\alpha Z_\alpha - Z_\alpha M_\delta]}{1845 M_\alpha} \tag{29}$$

and

$$w_z = (M_\alpha Z_\delta - Z_\alpha M_\delta)/Z_\delta \tag{30}$$

$$\omega_{AF} = \sqrt{-M_\alpha} \tag{31}$$

$$\zeta_{AF} = \frac{Z_\alpha \omega_{AF}}{2M_\alpha} \tag{32}$$

Similarly, the equation for θ can be written as,

$$\frac{\dot{\theta}}{\delta} = k_3(1 + T_\alpha s)/(1 + \frac{2\zeta_{AF}}{\omega_{AF}} s + \frac{s^2}{\omega_{AF}^2}) \tag{33}$$

$$K_3 = \frac{1845 K_1}{V_M} \tag{34}$$

$$T_\alpha = \frac{M_\delta}{M_\alpha Z_\delta - Z_\alpha M_\delta} \tag{35}$$

Chapter-4 Introduction to flight control Design

A simple flight control system (FCS) has three components with possibly many feedbacks to efficiently stabilize and govern the trajectory of the flight (Fig. 8). The three components are the autopilot(T1), the actuator(T2) and the missile airframe transfer function(T3). We have seen the internal workings and the derivations of the missile airframe TF in the last chapter. It is to be noted that we use the linearized TF in the flight control system for lower computational times.

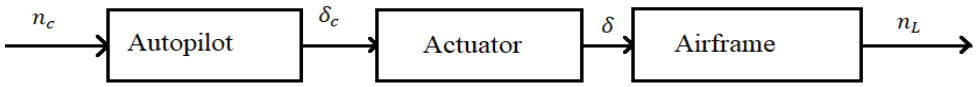

Figure 8: Open loop FCS

The simplest FCS is an open loop control simply allowing the signal to pass forward. This is the least expensive, but the output is slightly underdamped damped. In order to further elaborate on the above block diagrams, the TF for the Autopilot which is a relation between the desired acceleration and the required fin deflection can be obtained as a part from the previous derivation of the Missile airframe transfer function. It is given by the relation

$$n_c = \frac{1}{k_1}\,\delta_c \tag{34}$$

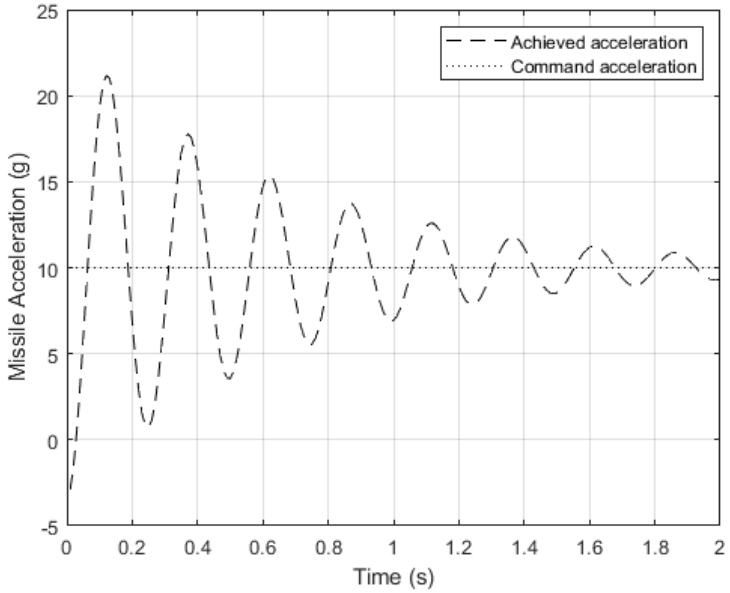

Figure 9: Open loop FCS Matlab plot at sea-level

Here, we the value of k_1 is integrated into T3 as,

$$n_L = \frac{k_1\left(1-\frac{s^2}{\omega_z^2}\right)}{1+\frac{2\zeta_{AF}}{\omega_{AF}}+\frac{s^2}{\omega_{AF}^2}}\delta \quad (35)$$

In the Fig. 8, the TF for the actuator is taken as 1, implying that we are neglecting the actuator effects. This block diagram upon programming in Matlab yields the following plots, as depicted in Fig.9. In this plot, the commanded and the obtained accelerations can be observed. It can be observed that for a given reference input of 10g, the resultant output finally stabilizes to the same value. Here, it has to be noted that the values of $\omega_{AF}, \zeta_{AF}, \omega_z, k_1$ are 25.3 rad/s, 0.058, 43.2 rad/s and -3.07g/deg respectively. However, there are significant modification which can be done to the TF block to reduce the settling time and the damping. One of them is presented below.

Rate-Gyro Flight Control System

In order to increase the low damping of the open loop flight control system, we can use a rate gyro to measure the missile body rate and feed this information back to develop the error signal. It is important to note that this FCS is more expensive than the open loop FCS and the feedback induces a stability problem which has to be effectively controlled.

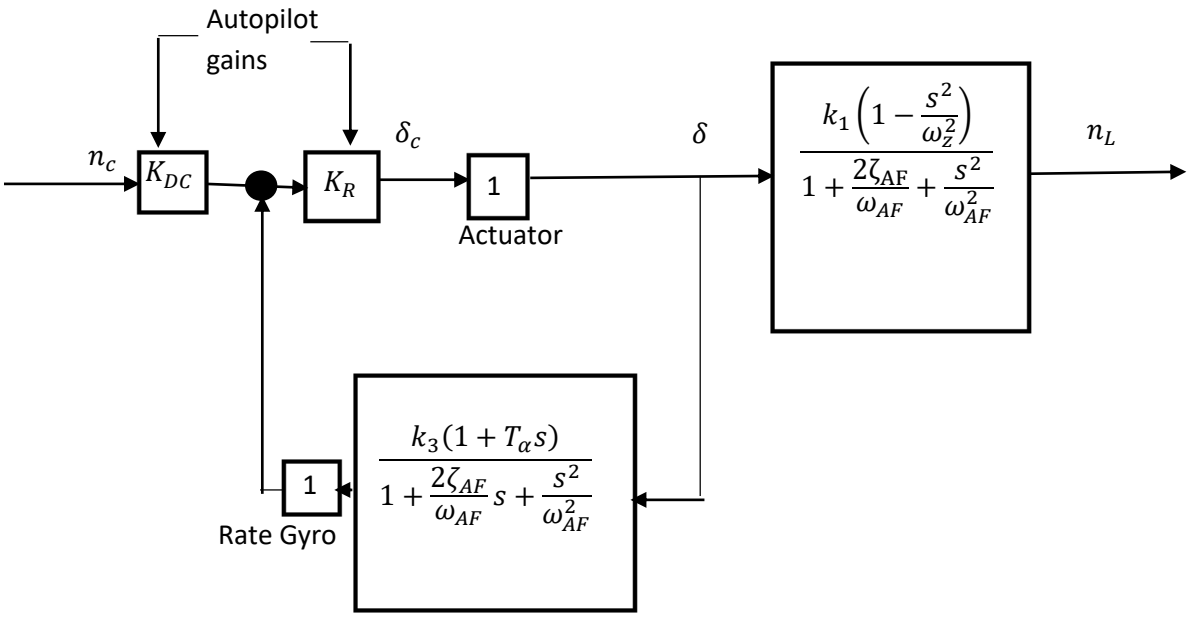

Figure 10: Rate Gyro FCS Block diagram

In Fig. 10, the terms hold their usual meanings as derived before, the new terms K_{DC}, K_R are the autopilot gains which are given by the equations below. The value of K_R is user defined.

$$K_{DC} = \frac{1-K_R K_3}{K_1 K_R} \quad (36)$$

The value of the autopilot gain (K_R) is crucial to stabilize the output signal. In order to comprehend this, two cases have been drafted below with different gains (K_R) and the outputs are observed in Fig. 11, 12.

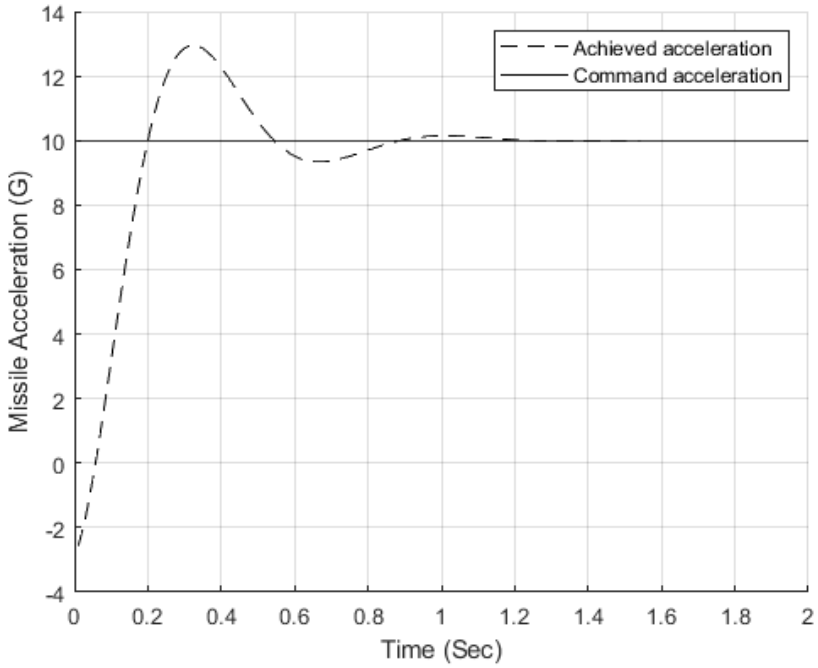

Figure 11: Acceleration with Autopilot gain K_R= 0.1

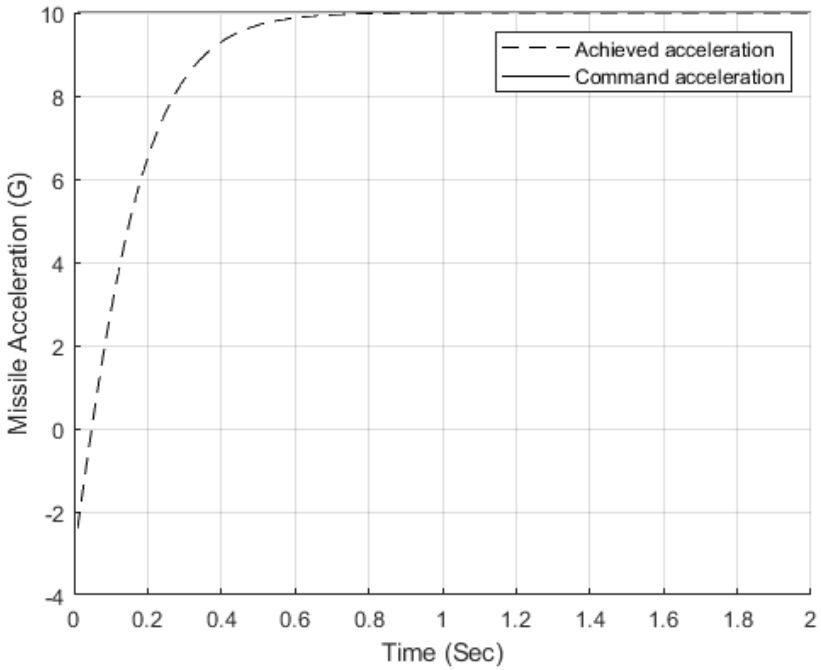

Figure 12: Acceleration with Autopilot gain K_R = 0.25

A critically damped case can be observed with an increased K_R, thus effectively stabilizing the output signal. It is to be noted that all the above calculations have been performed at an altitude of 15 Km.

Bode Plot Analysis

In order to understand the margins in which the system remains stable, a bode plot analysis has been done. Bode plots (Fig. 13) are drawn over the logarithmic scale of frequency and against the gain and the phase values.

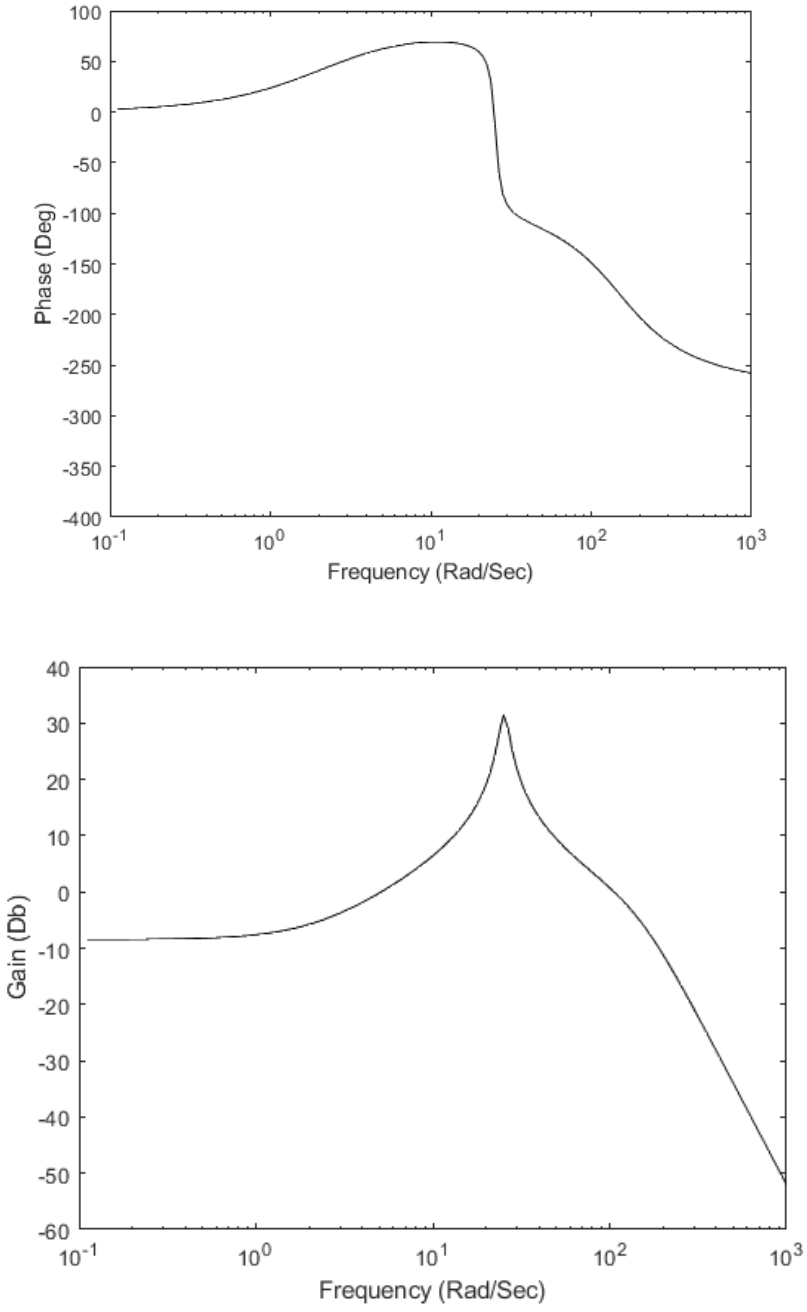

Figure 13: bode plot diagrams of the open loop FCS

The Gain crossover frequency is 150 rad/s and the phase crossover frequency is 64 rad/s. The phase margin is 55° and the gain margin is 11.5 dB. Increasing these operational parameters beyond this range would make the system unstable.

Building Simulink models

The previous sections describe the open loop FCS and the RG FCS. The advantages of one over the other are also presented. Both of them are built using Simulink block diagrams (Fig. 14).

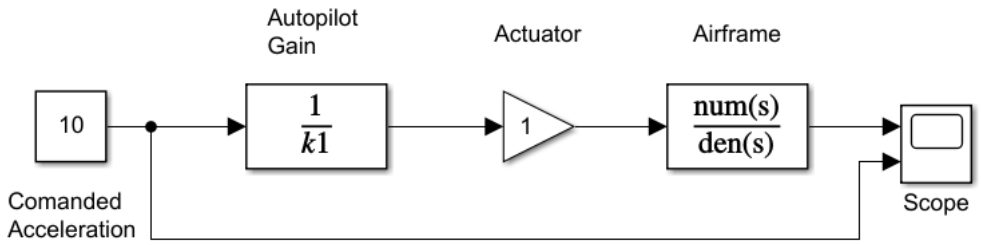

Figure 14: Open Loop FCS Block Diagram

The scope of the above block diagram gives the following plot (Fig. 15) which is similar to Fig.9.

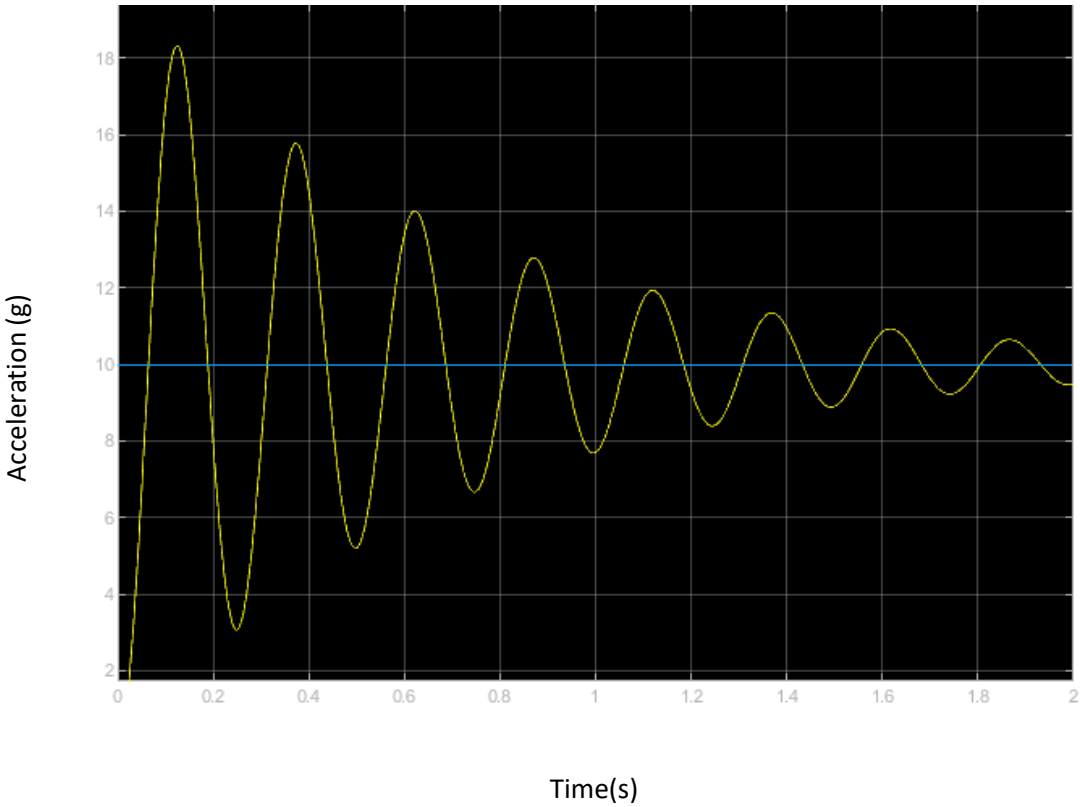

Figure 15: OLFCS output scope

The value of the Gain K_1 is -3.07 g/deg and the value other values of the constants in the AF TF are calculated to be $\omega_{AF} = 25.3\frac{rad}{s}$, $\zeta_{AF} = 0.058, \omega_z = 43.2\frac{rad}{s}$. The value of the AF TF is

$$\frac{k_1\left(1-\frac{s^2}{\omega_z^2}\right)}{1+\frac{2\zeta_{\mathrm{AF}}}{\omega_{AF}}+\frac{s^2}{\omega_{AF}^2}} \qquad (37)$$

Now, the Rate-gyro Flight control system is built in Simulink in the following manner as seen in Fig.16:

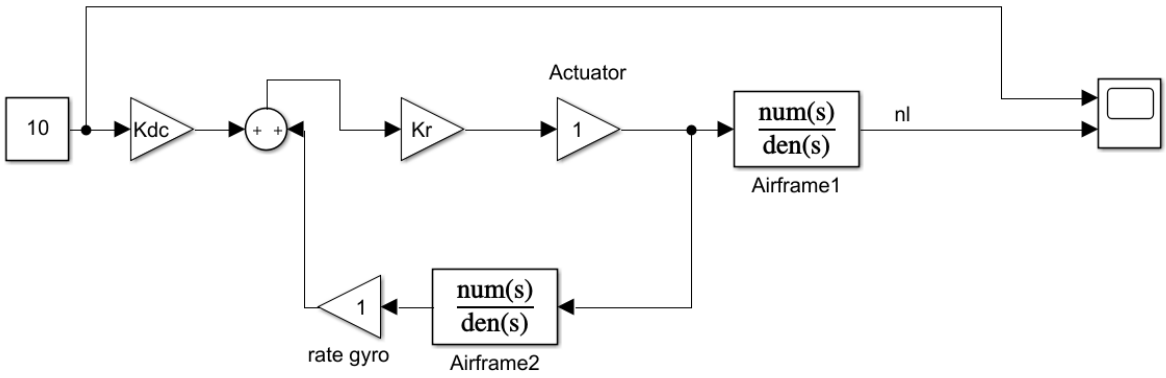

Figure 16: RateGyro FCS Block Diagram

It is important to note that the actuator dynamics has been ignored in this simulation as well. This is one of the drawbacks of these previous models which will be addressed in the three loop autopilot. Nevertheless, the values of the newly added (added to OLFCS) are as follows: $K_r = 0.1, K3 = -1.889, T_\alpha = 0.45$, plotted at sea-level.

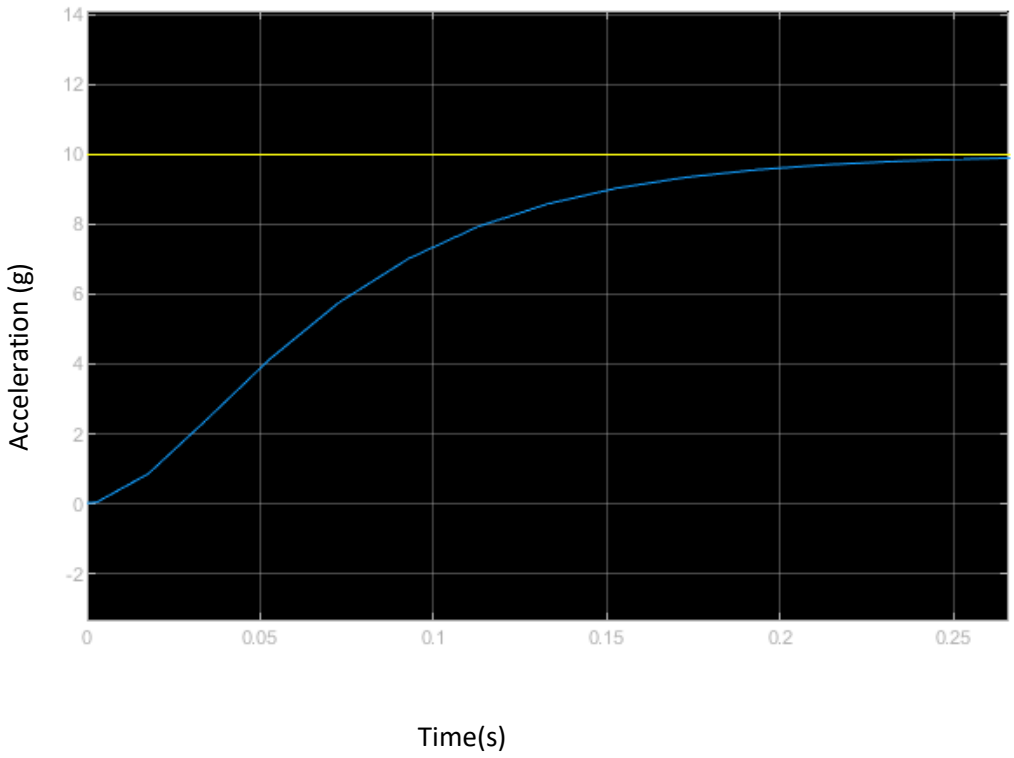

Figure 17: Acceleration over time in RGFCS

The value of the K_{dc} can be calculated as

$$\frac{1 - K_r K_3}{K_1 K_r} \tag{38}$$

Chapter-5 Three Loop Autopilot

The three loop Autopilot (TLAP) provides us with more freedom to dictate the hyper parameters of the overall equivalent TF of the missile. It contains an accelerometer which feeds back the obtained acceleration over the previously discussed RGFCS (as shown in Fig.18). Hence, it also has a rate gyro which feeds back body information to the input. It is important to note that the TLAP aids us with the ability to select independently the system damping (ζ), the time constant τ and the open loop crossover frequency (ω_{OLCF}).

The system damping makes sure that the missile is not overly sensitive to the Radome slope error. The Time constant is the time the system takes to reach 63% of the steady state value. With low, time constants the system can have better manoeuvrability. The ω_{OLAF} makes the system robust against un modelled frequencies.

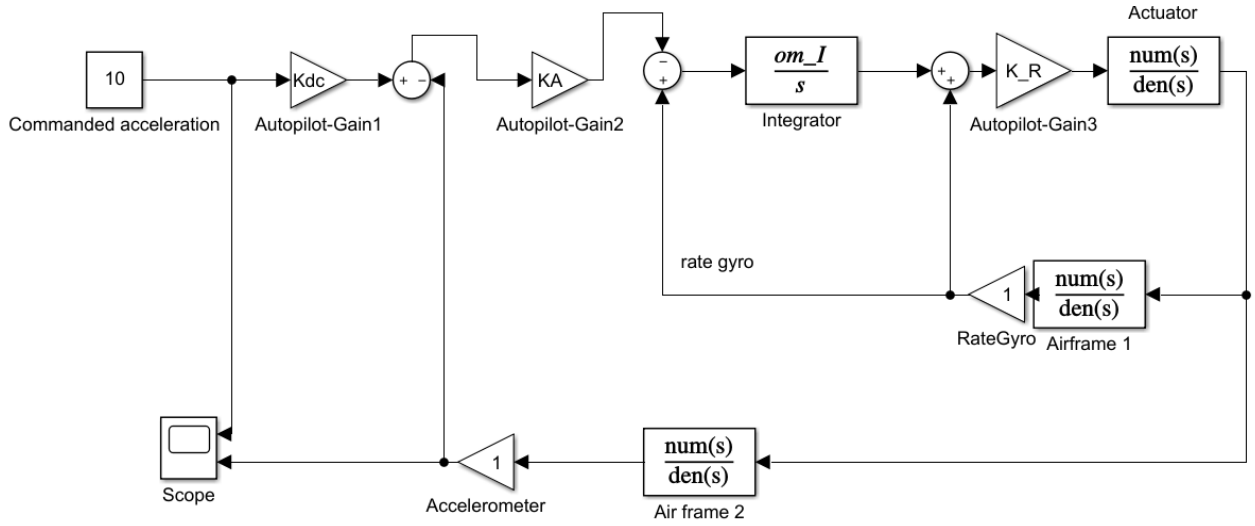

Figure 18: Three Loop Autopilot FCS Block Diagram

The above block diagram is built in Simulink, it is important to note the values of the Airframe1 and Airframe2. They are same as the ones which have been used in the RGFCS. However, it is important to note that the Actuator dynamics have also been added to the system. A simple second order system is added with a natural frequency of 150 rad/s and a damping coefficient (ζ_{ACT}) of 0.7. The block diagram of the actuator can be displayed as:

$$\frac{\delta}{\delta_c} = 1/(1 + \frac{2\zeta_{ACT}}{\omega_{ACT}}s + \frac{s^2}{\omega_{ACT}^2}) \quad (39)$$

It is important to note that there are a few unknowns in the block diagram above. The values of $K_{dc}, K_A, \omega_I, K_R$ are unknown. However, we know the set of desired parameters which we intent the system to have. (ζ, τ, ω_{OLCF}). Now, with open and closed loop analysis, we derive a set of equation for the unknown autopilot parameters, before we can operate on the block diagram. The following equations are derived:

$$K_{dc} = 1 + K_c \quad (40)$$

Where K_c is a gain which is defined a

$$K_c = \frac{-\left(\frac{\omega_o^2}{\omega_z^2}\right) - 1 + 2\zeta_o\omega_o T_\alpha}{1 - 2\zeta_0\omega_0 T_\alpha + \omega_o^2 T_\alpha^2} \tag{41}$$

Here,

$$\omega_0 = \frac{\omega}{\sqrt{\tau\omega_{CR}}} \tag{42}$$

and

$$\omega_{CR} = -\frac{K_0\omega_{AF}^2}{\omega_0^2} \tag{43}$$

In order to obtain our unknown parameters (K_A, ω_I, K_R) the following equation are used:

$$K_A = \frac{K_3}{K_c K_1} \tag{44}$$

$$\omega_I = \frac{T_\alpha K_c \omega_o^2}{1 + K_c + \frac{\omega_0^2}{\omega_0^2}} \tag{45}$$

$$K_R = \frac{K}{K_A\omega_I} \tag{46}$$

Where,

$$K = \frac{K_0}{K_1(1 + K_C)} \tag{47}$$

These equations are solved before substituting them in a transfer function in order to control the output. It is important to note that these variable remain constant throughout the time of the simulation. The input parameters: $\tau = 0.3s, \zeta = 0.7, \omega_{CR} = 50$ rad/s.

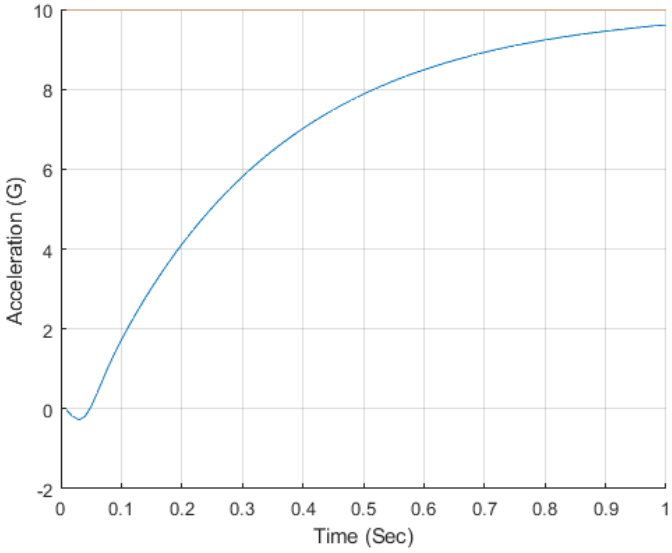

Figure 19: Output signal of the Three Loop Autopilot

This undershoot (as seen in Fig.19) of the achieved acceleration is a typical characteristic of non-minimum phase systems. In such systems, the overall transfer function has an unstable pole/zero. A certain time delay is associated with these systems.

Bode plot analysis of the open loop system

The Gain behaviour over a range of frequency:

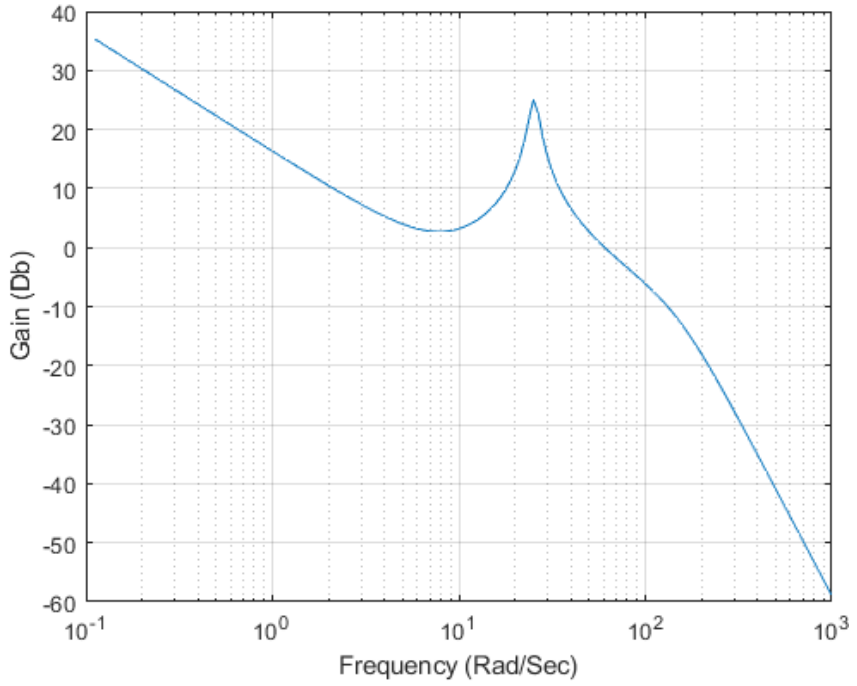

The Phase behaviour over a range of frequency:

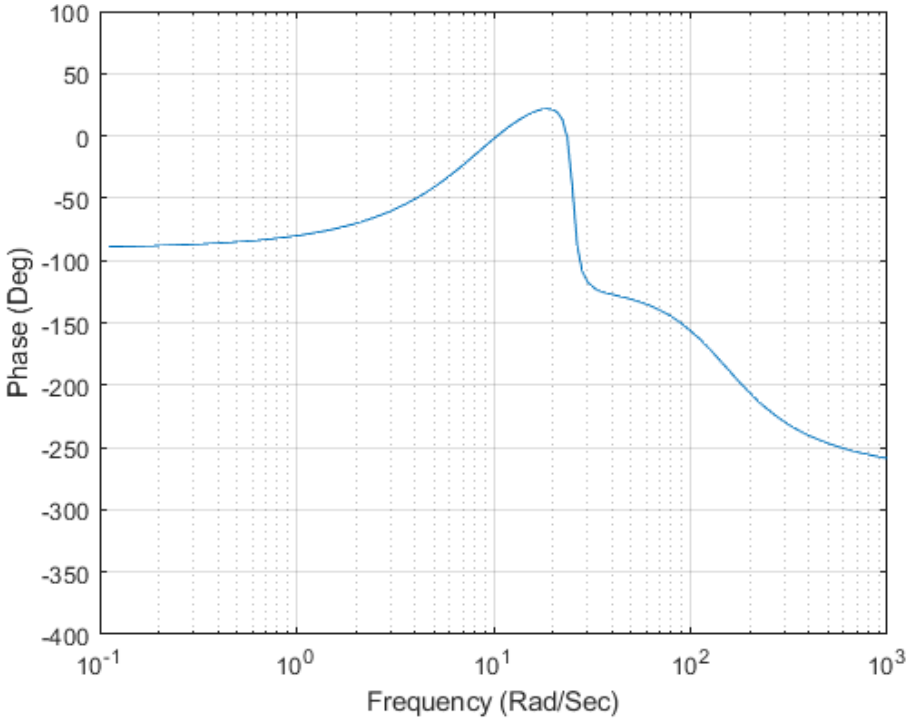

Figure 20: Bode plot analysis of TLAP FCS

It is to be noted that the open loop has been broken before the actuator for bode plots. From Fig, 17 the time constant of the system can be validated to be close 0.3s, which was our input parameter. The open loop crossover frequency (a.k.a Gain cross over frequency) can be verified from the bode plots to be 60 rad/s. It is close to out commanded value of 50 rad/s.

Three Loop Autopilot

The Model shown at the beginning of the chapter is built in Simulink. A time delay of ~0.34s is observed and the output it similar to the Matlab simulations. The scope of the block diagram displays the following graphs (Fig. 21):

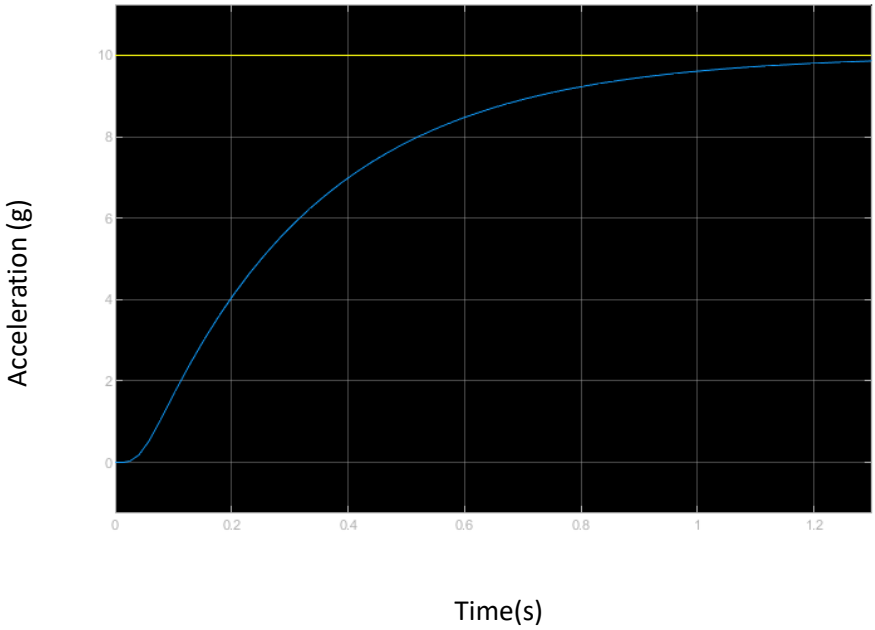

Figure 21: Simulink scope of the TLAP FCS

The Simulink model replicates the Matlab code precisely which can be compared to Fig. 19.

Chapter-6: Comparative study

Open Loop Flight Control system	Rate Gyro Flight Control system	Three Loop Autopilot System
Really cheaper when compared to the others: it is sufficient to just get the job done.	Moderately expensive when compared to the OLFCS, but cheaper than TLAP.	Very expensive.
The output signal is significantly under-damped, resulting in an 83% overshoot.	The output is critically damped and the overshoot has been completely eliminated.	The output is highly customizable and the overshoot can be completely eliminated.
The actuator and the accelerometer dynamics have been ignored.	The accelerometer and the actuator dynamics have been ignored.	A second order actuator dynamics has been assumed and the accelerometer has been assumed to be placed at the center of mass.
The transfer function user has very less control in order to manipulate the output of the system. The nature of the signal will depend on the operating conditions of the missile and cannot be physically altered. (K_1)	There are two autopilot gains which empower with more maneuverability to control the output of the missile. (K_{DC}, K_R) . K_R can be modified to make the system critically damped.	The time constant (τ), the damping coefficient (ζ) and the open loop cross over frequency (ω_{CR}) can be controlled by the user by varying the autopilot constants $K_{dc}, K_A, \omega_I, K_R$.
Minimum phase system	Minimum phase system	Non-minimum phase system (can be observed from the acceleration plots)

Open Loop Flight Control system	Rate Gyro Flight Control system	Three Loop Autopilot System
No external sensors are utilized in the feedback loops. (because no feedback loops!)	Utilizes to gyroscope to feed back the body rate of the missile.	Utilizes an accelerometer and gyroscope to feedback the achieved acceleration and the body rate back into the transfer function.
The damping coefficient ζ = 0.058.	The damping coefficient is equal to and τ = 0.085s and ζ=1.	The output nature is ζ = 0.7, τ = 0.34, ω_{CR} = 50 rad/s which can be customized.
Extremely sensitive to Radome slope error	Resistant to Radome slope discrepancies.	Resistant to Radome slope discrepancies.
Sensitive to un-modelled frequencies.	Sensitive to un-modeled frequencies.	Control of ω_{CR} gives the advantage to stabilize the system against un-modelled frequencies by controlling the gain and the phase margins.
Unreliable for practical applications.	Reliable under extremely controlled flight conditions.	Most feasible control strategy against alien flight conditions.

Chapter-7: Conclusions

Let us consider the case study in which we compare RGFCS and TAPFCS. In a RGFCS, without the actuator dynamics, the only controllable parameter is the autopilot gain (K_r). As the value of the K_r increases, the value of the time constant and the damping coefficient increase. An increase in the damping coefficient is desirable, but its side effect leading to an increase in the τ is not. The plots (Fig. 22, 23) below depict the output nature without the actuator dynamics.

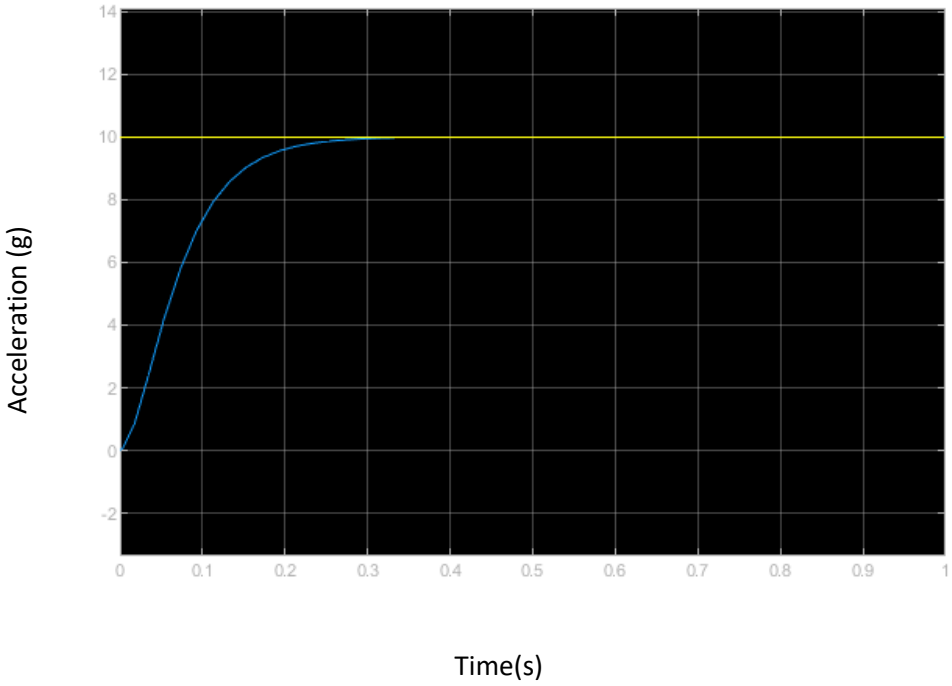

Figure 22: K_r = 0.4, τ = 0.09

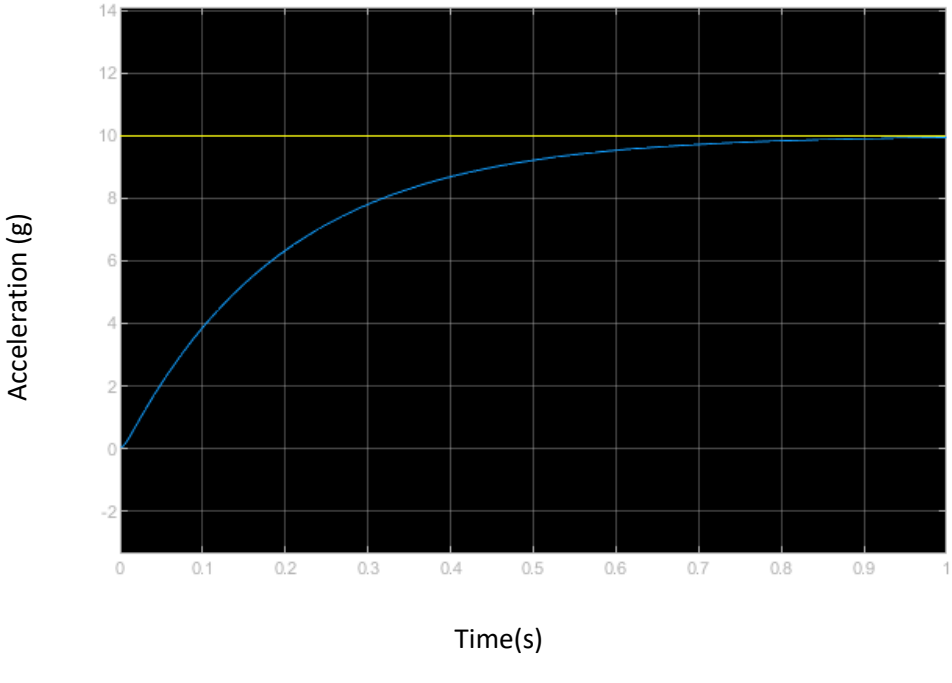

Figure 23:$K_r = 0.4$, τ =0.2

However, as the altitude increases the damping coefficient effectively decreases. One might assume that a continual increase in K_r should be sufficient to overcome the task. But, this wouldn't work in the presence of valid actuator dynamics as depicted in the plots (Fig. 24, 25) below:

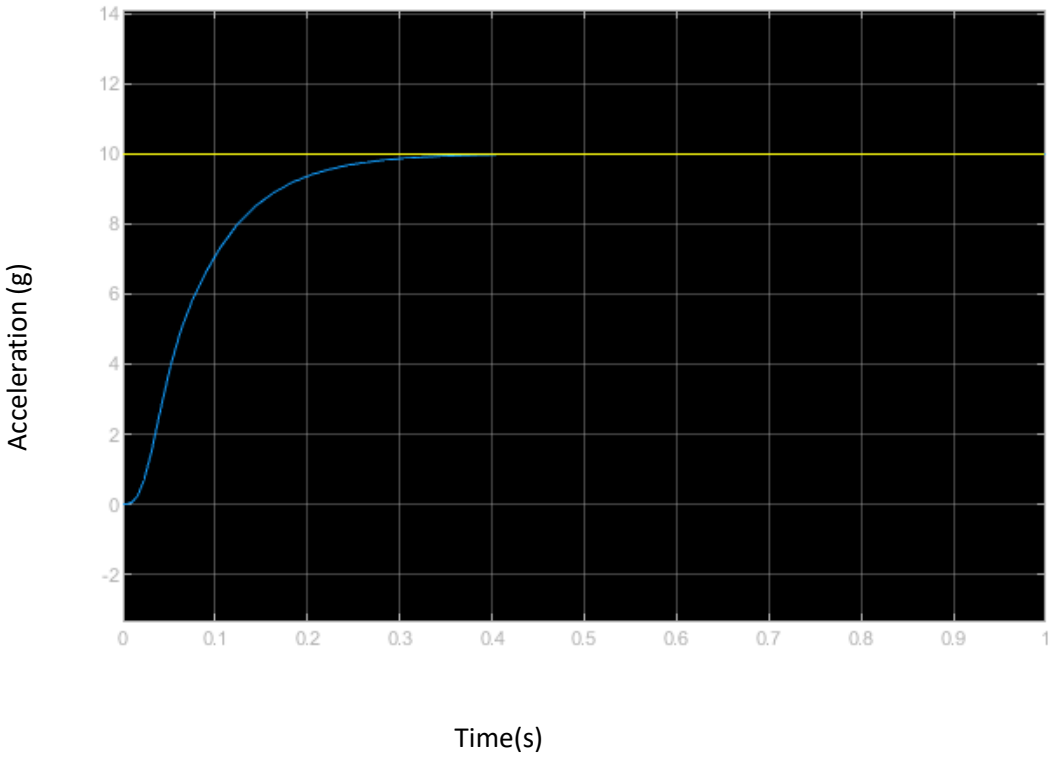

Figure 24: Considering actuator dynamics, K_r = 0.1

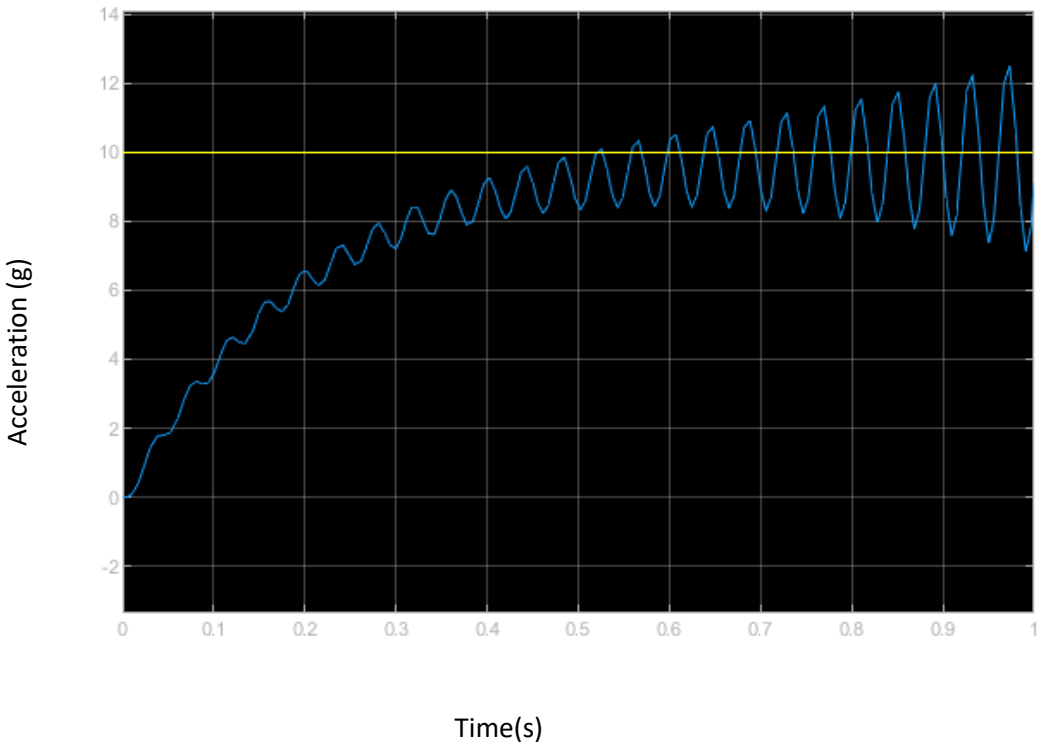

Figure 25: Considering actuator dynamics, K_r = 0.4

In order to control the time constant and the damping coefficient efficiently, the Three Loop Autopilot comes into the picture (Fig. 26). Here, the value of the open loop crossover frequency can be sabotaged to obtain the desired values for the τ and ζ.

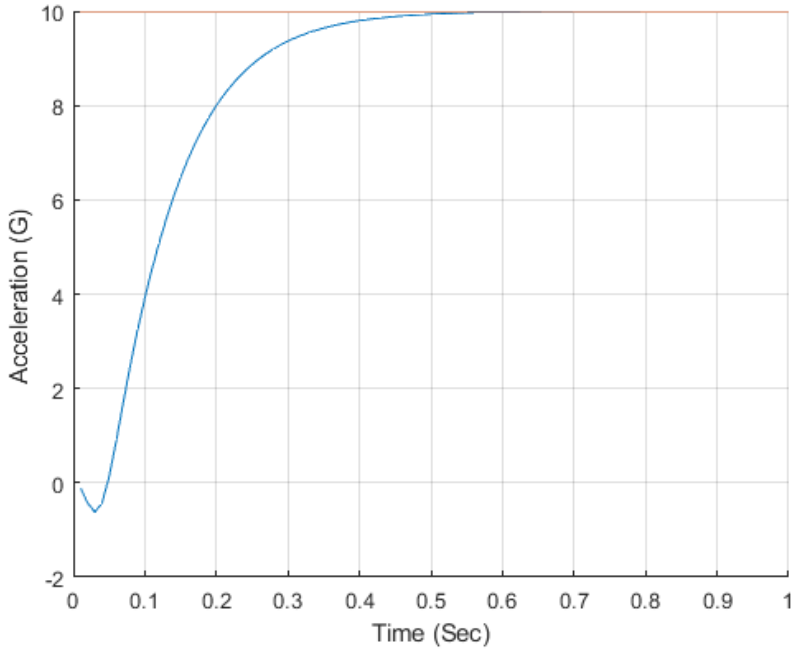

Figure 26: ω_{CR}= 50, $\tau = 0.13$, ζ= 0.7, ω_{act} = 150

In this system, as an example the time constant can be further reduced to (the input value) 0.03s, the following plot is observed (Fig. 27):

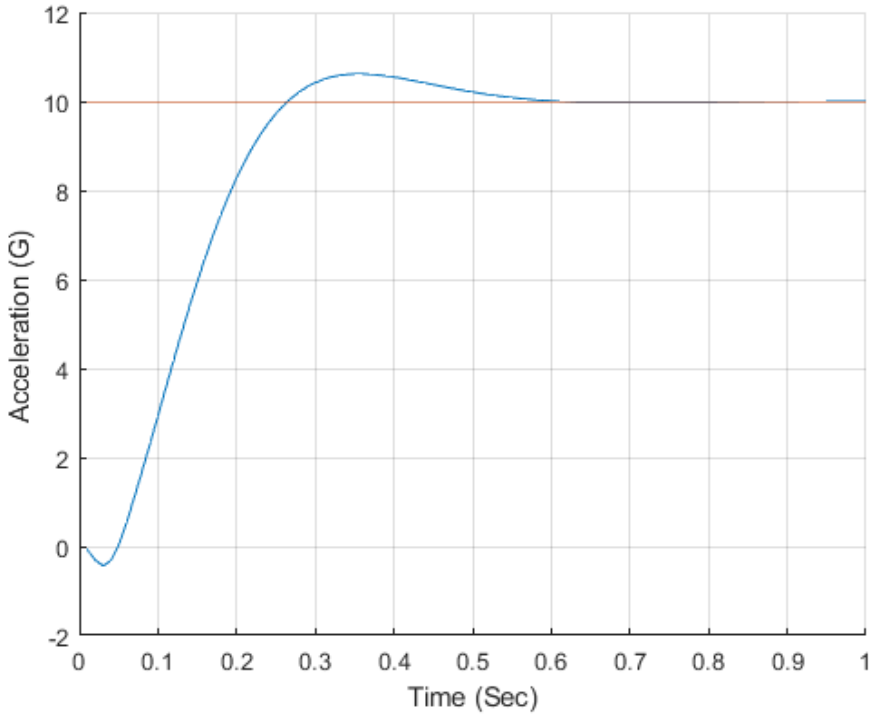

Figure 27 : ω_{CR}= 50, $\tau = 0.03$, ζ= 0.7, ω_{act} = 150

However, it can be seen that the time constant has not been satisfactorily achieved, to overcome this we now relax the ω_{cr} parameter to 100. Now, the following output (Fig. 28) is observed:

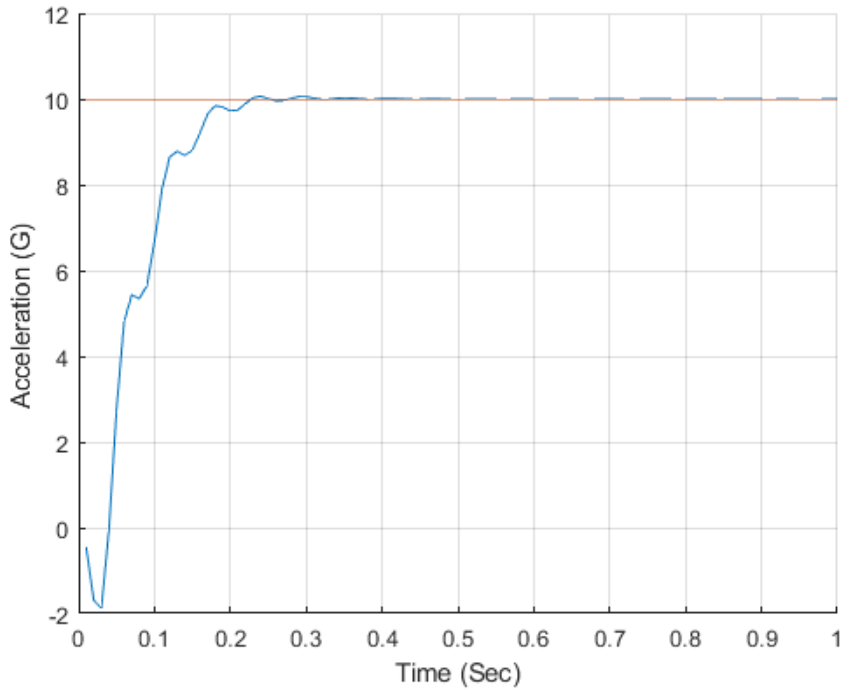

Figure 28: ω_{CR}= 100, $\tau = 0.03$, ζ= 0.7, ω_{act} = 150

Though, the τ has not completely been achieved, it is a considerable improvement. In order to improve the nature of this signal, the actuator bandwidth has to be increased (Fig. 29). (from 150 to 300 rad/s)

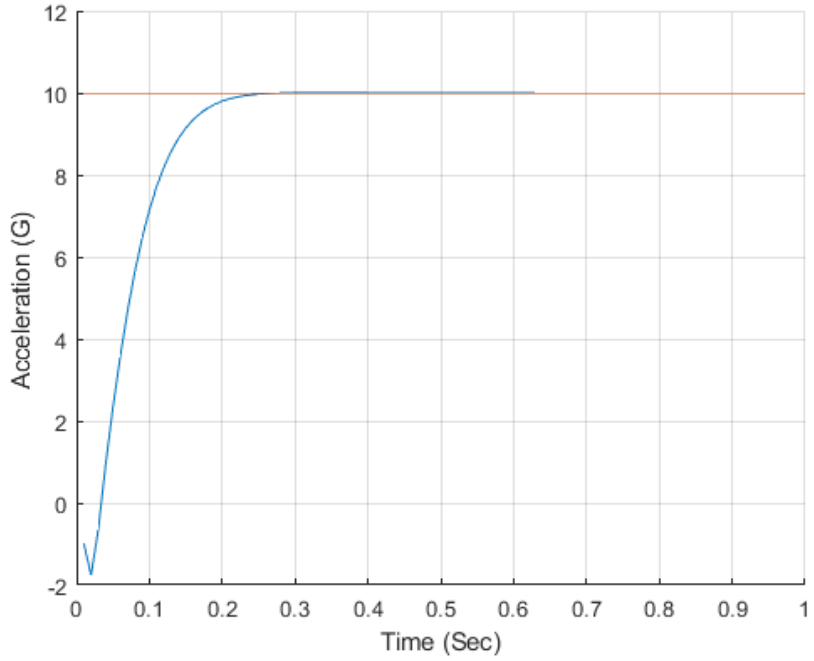

Figure 29: ω_{CR}= 50, $\tau = 0.03$, ζ= 0.7, ω_{act} = 300

This closely resembles the desired result of a low τ and a high ζ.

Based on the above comparative study, ignoring the Radome slope discrepancies, we can conclude that under extremely controlled flight conditions, the Rate Gyro Flight control system proves to be an optimal control strategy. However, considering the importance of the Radome slope errors and the robustness of the missile in un-modelled frequencies, the Three Loop Autopilot is the most efficient control strategy which seems to be pragmatic in real-world scenarios.

To conclude, the superiority of three loop autopilot flight control system can be explained in terms of the control over the different flight hyper parameters which it enables us to manipulate. The system damping makes sure that the missile is not overly sensitive to the Radome slope error. The ω_{OLAF} makes the system robust against un modelled frequencies.

References

[1] K. Ogata and Y. Yang, Modern control engineering., Prentice hall India,, 2002, vol. 4..

[2] P. Zarchan, Tactical and strategic missile guidance., American Institute of Aeronautics and Astronautics, Inc, 2012.

[3] D. H. Platus, "Ballistic Re-entry Vehicle Flight Dynamics," *Journal of Guidance,,* Vols. Vol. 5, Jan.–Feb. 1982, pp. 4–16..

[4] turkeywonk.wordpress. [Online]. Available: https://turkeywonk.files.wordpress.com/2013/11/figb-23.gif.

[5] g. s. Mathworks. [Online]. Available: https://in.mathworks.com/help/simulink/examples/designing-a-guidance-system-in-matlab-and-simulink.html.

[6] F. W. a. Z. P. Nesline, "A New Look at Classical Versus Modern Homing Guidance," *Journal of Guidance and Control,,* Vols. Vol. 4, No. 1, 1981, pp. 78–85.